First-principles study of the wurtzite-to-rocksalt phase transition in zinc oxide

2007 J. Phys.: Condens. Matter 19 266207

(http://iopscience.iop.org/0953-8984/19/26/266207)

IOP PUBLISHING JOURNAL OF PHYSICS: CONDENSED MATTER

J. Phys.: Condens. Matter **19** (2007) 266207 (12pp) doi:10.1088/0953-8984/19/26/266207

First-principles study of the wurtzite-to-rocksalt phase transition in zinc oxide

Jin Cai and Nanxian Chen

Department of Physics, Tsinghua University, Beijing 100084, People's Republic of China

E-mail: caijin@tsinghua.org.cn

Received 19 January 2007, in final form 8 May 2007
Published 7 June 2007
Online at stacks.iop.org/JPhysCM/19/266207

Abstract

Wurtzite (B4) compounds commonly undergo a structural transition to the rocksalt (B1) phase under high pressure. The underlying transition mechanism, or the so-called transition path, has been extensively investigated in recent years. Two different transition paths have been proposed for the B4–B1 phase transition, that is the 'hexagonal' path and the 'tetragonal' path. In this work, taking zinc oxide (ZnO) as an example, we have made a comparative study of these two paths from first-principles. The calculated results lead to the conclusion that the tetragonal path is more favourable under lower pressure but the hexagonal path is more favourable under higher pressure, which indicates a competition between these two paths in the ZnO case. We have also investigated the evolution of structural and electronic properties along the two different paths; the axial ratio c/a is suggested as a good indicator in experiments to identify the transition path.

(Some figures in this article are in colour only in the electronic version)

1. Introduction

Zinc oxide (ZnO) is a wide band gap semiconductor with a range of technological applications including electronic and electro-optic devices, catalysts, chemical sensors, solar cells, and surface acoustic wave devices [1–3]. As a typical semiconductor compound and an example in mineralogy, ZnO has also attracted interest because of its high-pressure behaviour in both experiment [4–11] and theory [11–15]. At ambient conditions, ZnO crystallizes in the wurtzite (B4, space group $P6_3mc$) phase and it goes through a phase transition to the rocksalt (B1, space group $Fm\bar{3}m$) phase at a pressure of ∼9 GPa [4–7]. Upon releasing the external pressure, a reverse transition from B1 to B4 has been reported at ∼2 GPa [6, 7], which shows a rather large hysteresis. Such a pressure-induced phase transition is very common for most of the wurtzite compounds. The underlying transition mechanism, i.e. the so-called transition path, has received much attention since it reveals the microscopic process of the phase transition and

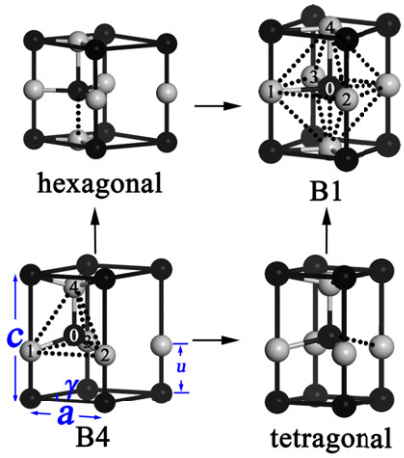

Figure 1. Schematic representation of the two different mechanisms proposed for the B4–B1 phase transition: one path through the 'hexagonal' intermediate structure, and the other through the 'tetragonal' one. The atom mapping relation is indicated by the numerals labelled in the B4 and B1 structures.

might lead to new experiments and possibly the control of transition processes. However, the B4–B1 transition mechanism has not been fully understood until now.

In previous studies, a series of models were proposed for the B4–B1 structural phase transition [16–27]. All these models can be summarized as two different transition paths (as shown in figure 1): one is the 'hexagonal' path and the other is the 'tetragonal' path. Along each of these two paths, the B4–B1 transition can be regarded approximately as a two-stage process. At the first stage of the hexagonal path, the fractional coordinate u changes from $\sim$0.38 to 0.50 accompanied with the compression of the axial ratio c/a from $\sim$1.6 to $\sim$1.2. The resulting 'hexagonal' intermediate structure is isomorphic to the layered h-BN. In this structure, each Zn (or O) atom is located at the centre of the equilateral triangle formed by three O (or Zn) atoms, and has two opposite bonds along the c axis, perpendicular to the triangle plane. Then in the next stage, the hexagonal angle γ opens from 60° to 90° and the Zn (or O) atom moves horizontally from the centre of the triangle to the centre of the square, thus the h-BN phase transforms into the B1 phase. On the other hand, there is an analogous deformation along the tetragonal path, but with the above two stages reversed. In this case, the γ angle at first opens up to 90° accompanied by the atoms moving horizontally to the square centre, while c/a and u increase slightly; each Zn (or O) is located at the body centre of a square pyramid formed by five O (or Zn) atoms. This results in a 'tetragonal' intermediate phase. The B1 phase is then obtained through a decrease of the c/a ratio, which simultaneously brings the Zn (or O) atoms from the body centre to the base centre of the pyramid. It is noticeable that the two mechanisms share the same atom mapping relation from the initial B4 phase to the final B1 phase (as illustrated in figure 1) though they are different in the cell deformations and atomic shifts.

The first comparative study of these two mechanisms was given by Saitta and Decremps [24] from the dynamical point of view, which leads to a conclusion that the wurtzite semiconductors containing d-electrons, such as ZnO, GaN, and InN, prefer the tetragonal path, but the hexagonal path is only possible for those containing light cations, such as AlN. However, the recent experiment by Liu *et al* suggests that the two possible mechanisms are in competition with each other, at least for ZnO. Thus, a more detailed study is needed to solve this puzzle and to improve our understanding of the B4–B1 structural transition.

In this work, based on first-principles calculations, we make a comparative study of these two kinds of mechanisms in the case of ZnO from the energetic point of view. The activation enthalpy, which corresponds to the maximum barrier height of the chemical enthalpy along a given transition path, is taken as the criterion to select the most probable path, i.e. the energy-favoured one. In particular, we pay much attention to the pressure dependence of the transition mechanism that was little discussed before. Then, the evolution of structural and electronic properties in the course of the transition process is investigated along the two different paths in order to search for a suitable indicator to monitor the transition process and possibly identify the actual mechanism in future experiments. The theoretical methods and computation details are presented in section 2. Section 3 contains the results and discussion. Section 4 is the summary of the present work.

2. Method and computation details

2.1. First-principles calculation

In this work, the first-principles calculations were carried out within the density functional theory (DFT), using the local density approximation (LDA) for the exchange and correlation potential implemented in the VASP code [28]. The electron–ion interaction was described using Vanderbilt's ultrasoft pseudopotentials [29]. Zinc 3d electrons were treated as valence electrons. The valence electronic wavefunctions were expanded in a plane wave basis set up to a kinetic energy cutoff of 400 eV. The Brillouin zone integrations were performed by sampling on gamma centred Monkhorst–Pack [30] grids with a $7 \times 7 \times 4$ division of the reciprocal unit cell.

2.2. Potential energy surface

The theoretical approach is very appealing to reveal the structural transition mechanism because of the difficulties of real-time measurements to monitor the fast transition process in experiments. A particularly fruitful method is to regard the phase transition process as a concerted movement of all atoms in the system on a high-dimensional potential energy surface (PES) [31]. The PES is defined as a hypersurface $H = H(\Omega)$, where Ω is the free structural parameter set and $H(= E + PV)$ is the chemical enthalpy as a function of Ω. Once the PES is obtained, it can be used to determine several points of interest such as the local minima (corresponding to stable or metastable states) and the saddle points (corresponding to transition states). Also, the PES can be used to search the energy-favoured transition path. As usual [32], the path is continuously traced back from the saddle point in the steepest descent direction to the minima to see whether they do correspond to the desired pair of end phases. Then the obtained path clearly represents the energy profile of the phase transition, the atomic shifts and cell deformations occurring during the phase transition process. These theoretical results can be compared with phenomenological kinetic data and provide a useful test-bed for future experimental developments.

For the B4–B1 transition, as illustrated in figure 1, the corresponding structural parameter set Ω consists of six parameters (a, c, γ, u, v, δ), where the parameters a and c are the cell edges and γ is the base angle. The parameter u is the relative displacement of the Zn and O sublattices along the c axis, i.e. in the direction of [001]; δ defines the relative displacement of the Zn and O sublattices in the direction of [110], and v relates to the relative sliding of the two adjacent (001) planes of the Zn (or O) sublattice also in the [110] direction. Note that in the commonly mentioned four phases shown in figure 1, δ is always equal to zero; however,

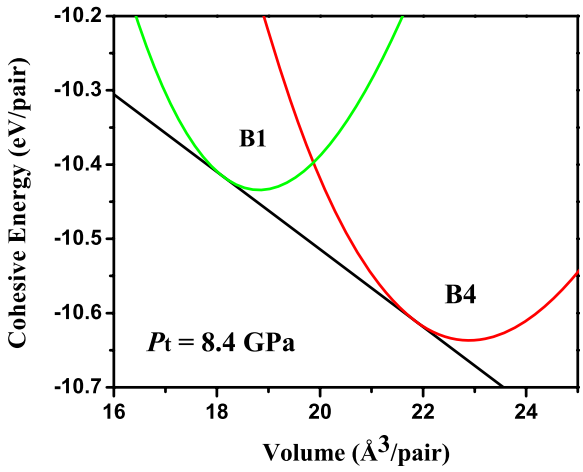

Figure 2. Cohesive energy as a function of volume for the B4- and B1-ZnO. The equilibrium transition pressure P_t is estimated at about 8.4 GPa from the common tangent construction.

in other phases along the transition paths, δ may deviate from zero a little. Thus, the origin (0, 0, 0) is occupied by one atom, and the fractional coordinates (δ, δ, u), (v, v, 0.5), and ($v - \delta$, $v - \delta$, $u + 0.5$) describe the positions of the other three atoms respectively. The free parameter set defines the symmetry restriction $Cmc2_1$ for both the tetragonal and the hexagonal paths [25, 26]. There are some other mechanisms which can be regarded as a modification of the $Cmc2_1$ case [26, 27], and the only difference is the arrangement of the four-atom unit cells to build up the crystal [26].

Now, we know that the complete PES of the B4–B1 transition is defined as a six-dimensional (6D) hypersurface. Obviously, it is not an easy task for first-principles calculations so it is necessary to introduce some simplifications. As shown in figure 1, the parameters γ and u can distinctly characterize the difference between the hexagonal path and the tetragonal one. So, instead of the 6D PES, we may calculate a two-dimensional (2D) PES $H(\gamma, u)$ by fixing γ and u and minimizing the enthalpy with the other parameters fully relaxed. The computational details are as follows. The variable range is defined as $(\gamma, u) = (57.5°, 92.5°) \times (0.37, 0.51)$, which covers the initial B4 phase (corresponding to (60.0°, ∼0.375)) and the final B1 phase (corresponding to (90.0°, 0.50)). We divided the γ–u space with a 15 × 15 mesh grid, and at each grid point, the parameters a, c, v, and δ were fully relaxed to reach the enthalpy minimum. The conjugate gradient algorithm was used for the energy minimization. After obtaining the data of the 15 × 15 mesh grid, the PES $H(\gamma, u)$ can be figured out as a contour graph by using the spline interpolation method to obtain smooth isolines.

3. Results and discussion

3.1. Transition mechanism

At the beginning, we need to calculate the equilibrium transition pressure P_t that is defined as the pressure at which the enthalpy of the initial (B4) phase is equal to that of the final (B1) phase. The value of P_t is mostly estimated from the common tangent of the energy–volume curves of the two end phases. Figure 2 shows the calculated energy–volume curves of the B4 and B1 ZnO structure, and the common tangent construction gives a P_t value of about 8.4 GPa.

Table 1. Calculated and experimental static properties for a ZnO crystal at zero pressure (some of the values at the transition pressure P_t are also given in square brackets). V denotes the equilibrium volume, E_{coh} denotes the cohesive energy, and B denotes the bulk modulus. For the calculated value, P_t denotes the equilibrium transition pressure (as defined in the text); and for the experimental value, it denotes the pressure corresponding to the experimental onset of the phase transition. $\Delta V/V_0$ is the relative change of volume from B4 to B1 of ZnO, where V_0 is the volume of B4-ZnO at zero pressure.

	Calculated		Experimental	
	This work	Reference [23]	Reference [6]	Reference [7]
	Wurtzite (B4)			
V (Å^3/pair)	22.91 [21.88]	22.8 [21.8]	23.81	23.796 [22.773]
E_{coh} (eV/pair)	10.637 [10.610]	10.64 [10.61]		
B (GPa)	160.5	162	142.6	183
	Rocksalt (B1)			
V (Å^3/pair)	18.78 [18.14]	18.7 [18.0]	19.60	19.484 [18.8]
E_{coh} (eV/pair)	10.434 [10.417]	10.43 [10.42]		
B (GPa)	210.5	210	202.5	228
	B4–B1 phase transition			
P_t (GPa)	8.4	8.22	9.1	8.7
$\Delta V/V_0$ (%)	18.0 [16.7]	18.0 [16.7]	17.7 [16.7]	18.1 [17]

These two energy curves also give some other static properties of ZnO, such as the equilibrium volume, cohesive energy, bulk modulus, and the relative change of volume from B4 to B1, which are listed in table 1 together with the previous calculated and experimental results for comparison. Overall agreement is obtained. This encourages the subsequent calculations to investigate the microscopic mechanism, which requires huge computational effort to acquire the potential energy surfaces.

As explained in section 2.2, the 2D potential energy surface $H = H(\gamma, u)$ is used to explore the B4–B1 phase transition (quasi-static) process in the present work. To study the pressure effect on the transition mechanism, we have calculated the PES at five different pressures: the ambient pressure ($\sim$1 bar $= 10^{-4}$ GPa), 4.0 GPa, the transition pressure (8.4 GPa), 10.0, and 15.0 GPa. Three of them are separately shown as a contour graph in figure 3. On these contour graphs, each (local) minimum point corresponds to a stable/metastable state and each saddle point corresponds to a transition state as a link with two adjacent stable/metastable states. Starting from the saddle point and continuously tracing in a downhill direction to the two adjacent minima points, one can obtain a transition path from the initial to final phases. All these typical states are marked in the contour plots and they are connected by dashed lines as a guide to the hexagonal or tetragonal transition path. Here, we introduce a rule of symbols as follows. The transition state and metastable state are abbreviated as 'TS' and 'MS' respectively; and 'h' or 't' are used as subscripts to denote the case of the hexagonal or tetragonal path. Further, there may be two transition states along one single transition path because of the existence of a metastable state between the B4 and B1 states. They are labelled using an arabic numeral (1 or 2). As an example, 'TS_h1' denotes the first transition state along the hexagonal path. In table 2, we list the corresponding structural parameters of all these typical states together with their enthalpies. Now, we are going to compare these two transition paths based on the calculated PES values.

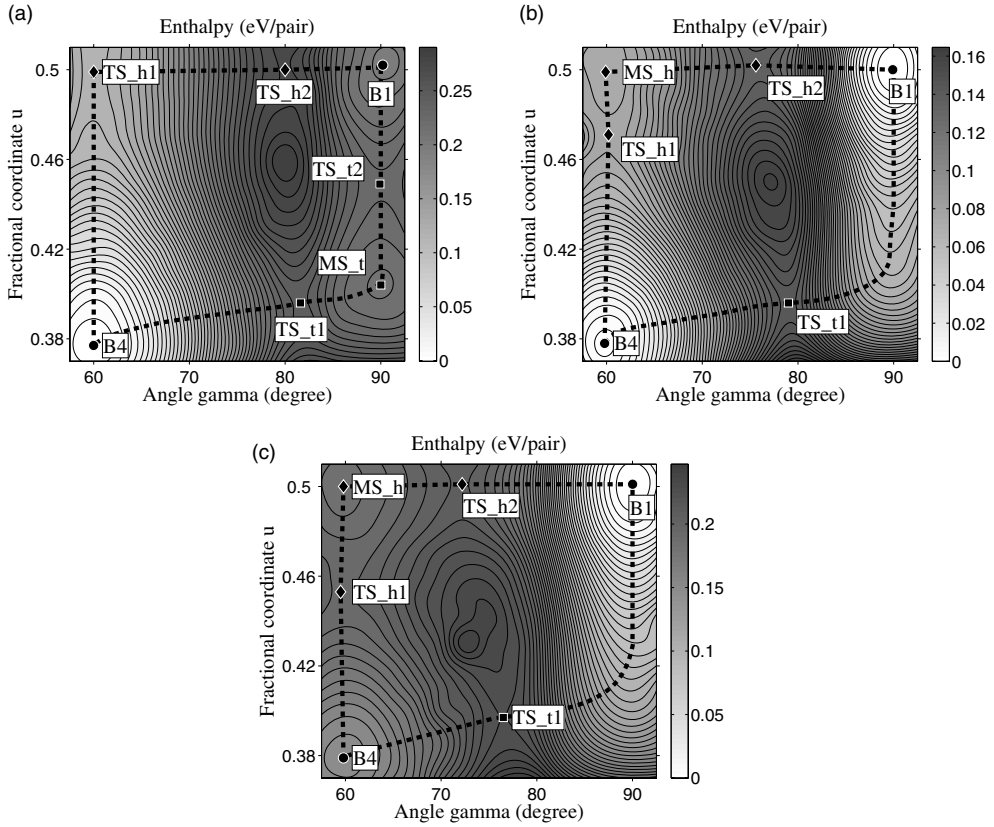

Figure 3. Contour plots of the minimized enthalpies of ZnO as a function of γ and u at (a) ambient pressure (∼1 bar), (b) equilibrium transition pressure (∼8.4 GPa); (c) 15 GPa. The dashed lines are shown as a guide to the hexagonal or tetragonal paths.

From the potential energy surfaces, it can be seen that the ZnO system needs to cross over some enthalpy barriers to accomplish the B4–B1 phase transition. The maximum barrier height ΔH along the transition path defines the corresponding 'activation enthalpy', which is the least cost crossing over the enthalpy barriers to accomplish the phase transition. As highlighted in table 2, the activation enthalpies of the hexagonal and the tetragonal paths are defined by the enthalpy values of TS_h2 and TS_t1, respectively, regardless of the various external pressures. By comparing the activation enthalpies, we can pick out the energy-favoured transition path. From the data given in table 2, the activation enthalpy of the tetragonal path is smaller than that of the hexagonal path in the lower pressure range; however, their activation enthalpies are comparable to each other in the transition pressure range, and the hexagonal path has a relatively low activation enthalpy in the higher pressure range. Therefore, we suggest that these two paths are competitive for the ZnO B4–B1 phase transition and the tetragonal one is preferable under lower pressure but the hexagonal one is under higher pressure.

The present calculated results indicate that the choice of the energy-favoured path for the B4–B1 transition might be affected by the external pressures in the case of ZnO. To our knowledge, this kind of pressure dependence was little discussed in previous theoretical studies of the B4–B1 phase transition. Saitta and Decremps (S&D) [24] investigated the pressure dependence of the elastic constants and predicted that ZnO transforms from B4 to B1 along

Table 2. Selected points of interest on the potential energy surfaces for ZnO calculated at five different pressures. The transition state and the metastable state are abbreviated as 'TS' and 'MS' respectively. A postfix of 'h' or 't' is used to denote the case of the hexagonal or tetragonal path; and an arabic numeral (1 or 2) is added as an index of the transition state along one single transition path. The parameter set (γ, u) of each point is given together with the corresponding enthalpy ΔH (with respect to the B4 state). The bold font highlights the activation enthalpy for the hexagonal or tetragonal path at a given pressure.

	B4	TS_h1	MS_h	TS_h2	TS_t1	MS_t	TS_t2	B1
				ZnO@1 bar				
γ (deg)	59.9	60.0		80.0	81.6	90.0	89.9	90.5
u	0.377	0.499		0.500	0.396	0.404	0.449	0.504
ΔH (eV/pair)	0.000	0.120		**0.274**	**0.246**	0.214	0.228	0.200
				ZnO@4.0 GPa				
γ (deg)	60.1	60.5		78.6	80.1	90.0	90.0	90.3
u	0.380	0.500		0.498	0.394	0.416	0.434	0.503
ΔH (eV/pair)	0.000	0.096		**0.201**	**0.191**	0.140	0.142	0.100
				ZnO@8.4 GPa				
γ (deg)	59.8	60.2	59.9	75.6	79.0			89.9
u	0.378	0.471	0.499	0.501	0.396			0.500
ΔH (eV/pair)	0.000	0.074	0.071	**0.135**	**0.141**			−0.002
				ZnO@10.0 GPa				
γ (deg)	60.3	60.2	60.0	74.7	78.4			89.9
u	0.378	0.464	0.500	0.502	0.395			0.501
ΔH (eV/pair)	0.000	0.067	0.063	**0.113**	**0.125**			−0.038
				ZnO@15.0 GPa				
γ (deg)	59.8	59.5	59.8	72.2	76.5			90.1
u	0.379	0.453	0.500	0.501	0.397			0.501
ΔH (eV/pair)	0.000	0.047	0.035	**0.058**	**0.077**			−0.151

the tetragonal path instead of the hexagonal one, which was suggested by Limpijumnong and Jungthawan (L&J) [23]. It is worth mentioning that both of these groups seem to have obtained the hexagonal and the tetragonal paths in their studies of the ZnO B4–B1 transition but they did not clearly notice the pressure dependence therein. As shown in figure 3 of [23], L&J calculated the PES for the B4–B1 phase transition of ZnO at the transition pressure P_t. Though their PES was defined with a structural parameter set different from ours, there are also two possible paths shown in their PES which are really consistent with the two paths discussed in the present work. Also, the structural configurations corresponding to the energy barriers are quite close to our results as shown in figure 3(b). In another work given by the group of S&D [9], first-principles calculations were performed to investigate the structural stability under elevated pressures and it was found that ZnO changes from B4 to MS_h at about 24 GPa (figure 11 of [9]). This implies a possible preference of the hexagonal path (under a relatively high pressure). Therefore, the previous theoretical studies have lent some support to the competition between the hexagonal and tetragonal path for the B4–B1 transition of ZnO. Besides, the present calculated results also show that it is not definitive for the preference of the transition path whether d electrons are contained in the concerned system or not, which was argued by S&D in [24]. The full electrons might make a coherent effect on this point, which needs further study in future work.

On the experimental side, Liu *et al* carried out an experiment in ZnO to study the pressure dependence of the internal structural parameter u by using high resolution angular dispersive x-ray diffraction [33]. In their experiment, u increases with pressure up to about 0.430 at around 5.6 GPa, and then rapidly decreases to about 0.38 before the onset of the phase transition. According to the $u(P)$ trend, they suggested that the hexagonal path is the preferred one up to 5.6 GPa, whereas it is in competition with the tetragonal path in the transition pressure range. Our present calculated results have confirmed the competition between the hexagonal and the tetragonal paths in the ZnO case. However, the tetragonal path is suggested as the most probable one in the lower pressure range, which is contrary to the analysis results of Liu *et al*. There is another puzzle among the experimental results and theoretical models. Along the hexagonal path, the axial ratio c/a will decrease from $\sim$1.6 to $\sim$1.2 and u will increase from $\sim$0.38 to 0.50, which is not completely consistent with the experimental results of Liu *et al*. In their experiment, the axial ratio c/a slightly decreases with pressure before the onset of transition, which is consistent with Desgreniers's experiment [7]. However, the obvious increase of u with pressure was not observed in the experiments of [7] and [9]. There seems to be a need for further experiments to clarify these issues. A key point here is that, in our view, the previous experimental results were reports of small compression behaviour in a volume before the onset of the phase transition, which cannot reasonably be compared with the theoretical models for the description of the structural transition process. This idea will be discussed again in the next subsection.

Also, one might be curious about what the pressure dependence of the transition mechanism means for ZnO. We would like to consider this problem in two respects. First, as shown in table 2, the activation enthalpy ΔH decreases with increasing pressure. Thus it can be seen from the Arrhenius factor $\exp(-\Delta H/k_{\mathrm{B}}T)$ that a lower activation enthalpy, i.e. a higher pressure, is necessary for the phase transition under lower temperature, and on the contrary, a higher activation enthalpy, i.e. a lower pressure, might be enough for the phase transition under higher temperature. Combining this with the pressure dependence of the two transition paths discussed in this work, we suggest that experiments at low T and high P might be appropriate to explore the hexagonal path. However, experiment at high T and low P might be appropriate to explore the tetragonal path. The second point is more interesting. As reported in experiment, the B4–B1 phase transition of ZnO is a reversible process. The forward transition takes place at about 9 GPa and the backward transition begins at about 2 GPa. Again from the pressure dependence of the transition mechanism, we make a conjecture here that the B4 phase of ZnO transforms into the B1 phase mainly along the hexagonal path but along the tetragonal path instead when it recovers to its ambient phase.

3.2. Structural and electronic properties

In section 3.1, we have obtained the transition paths from the potential energy surfaces and found that the two transition paths proposed previously are competitive for the ZnO B4–B1 phase transition. It is also very appealing to identify, with the aid of experiment, which mechanism is the preferred one. To shed light on this issue, we will have a look at the evolution of the structural and electronic properties of ZnO along the two different transition paths. The following calculations are performed at the equilibrium transition pressure 8.4 GPa only.

Figure 4 shows the contour graphs of the axial ratio c/a and the fractional coordinate v as a function of u and γ, which correspond to the PES of figure 3(b). The two possible transition paths are also outlined in the contour graphs. This clearly exhibits the evolution of the structural parameters along the corresponding path.

As shown in figure 4(a), the c/a ratio decreases first and then increases along the hexagonal path, whereas it increases slightly at first and then decreases along the tetragonal path. That is

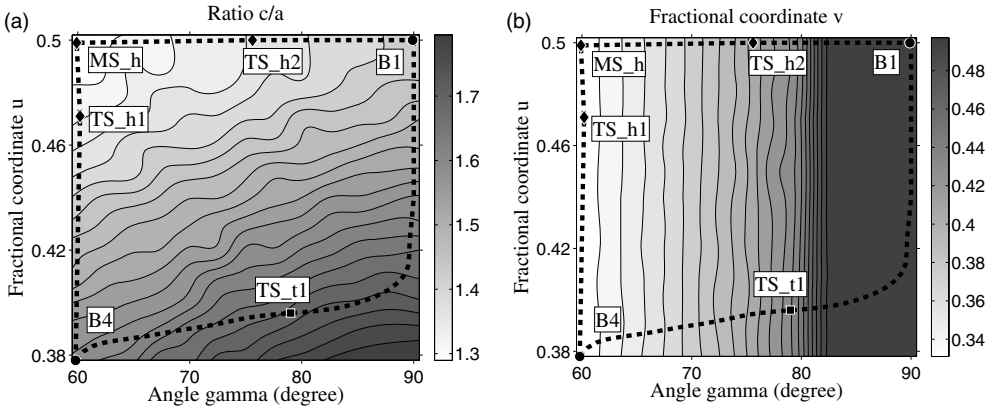

Figure 4. Contour plots of (a) the axial ratio c/a and (b) the internal coordinate v as a function of u and γ for ZnO calculated at the transition pressure 8.4 GPa. The typical states of the hexagonal and tetragonal paths are marked by diamonds and squares, respectively. The dashed lines linking these states outline the corresponding transition paths.

to say, the variation behaviour of c/a is quite different along these two paths, which implies that the measurement of the c/a ratio is a suitable choice to identify the hexagonal or tetragonal path in experiments. However, there is a need for real-time measurement *during* the transition process. The deformation of the structure mainly takes place in a very short time range near the transition pressure, which is not easily captured in current experiments. The fast transition process brings forward a challenging problem on the high time-resolving power for real-time observations in experiments. Most of the previous experimental studies focused on the change of structural parameters with increasing pressure *before* the onset of the phase transition, which is not the case discussed here.

On the other hand, the parameter v, as shown in figure 4(b), changes monotonically along both paths. Obviously, the structure parameters u and γ also change monotonically along both paths. Thus, compared with the case of c/a, measurements of any one of the parameters v, u, and γ might not reveal particularly significant differences between the two paths. It is also very interesting that the change of v almost depends upon the γ angle only, even in the full contour graph; see figure 4(b). This implies a strong coupling between the coordinate v and the angle γ.

Once the evolution of the structural parameters during the phase transition has been determined, the corresponding changes of the electronic properties can be investigated based on some additional first-principles calculations. Here we also adopt the DFT–LDA framework. Figure 5 shows the Brillouin zone and the related high-symmetry k-points used in the electronic structure calculations. We have calculated the band structures of six representative states on the transition paths, as shown in figure 6. There are two important features to note as follows.

First, along the two different paths, those phases corresponding to the same or comparable γ-angle size are of essentially identical band structures (in particular around the Brillouin-zone centre). For example, both B4 and MS_h (with the angle γ of 60°) are direct band gap semiconductors whereas both B1 and MS_t (with the angle γ of 90°) are indirect band gap semiconductors; and along either transition path, the direct–indirect transition takes place approximately at the barrier point, i.e. TS_h or TS_t (with the angle γ close to 80°). It can be said that the band structure is mainly affected by the angle γ but is not sensitive to the parameter u, which is very similar to the behaviour of the internal coordinate v as shown in figure 4(b).

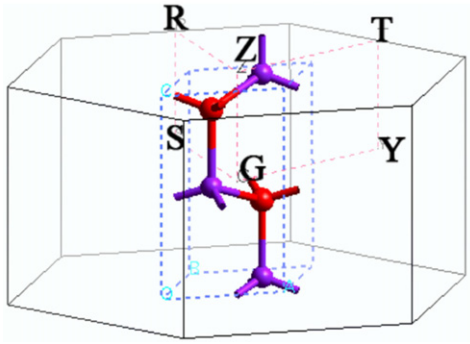

Figure 5. Brillouin zone of B4-ZnO. Applying appropriate distortions to the B4 cell will result in the corresponding Brillouin zone and high-symmetry k-points for the cell of B1 or any other intermediate state.

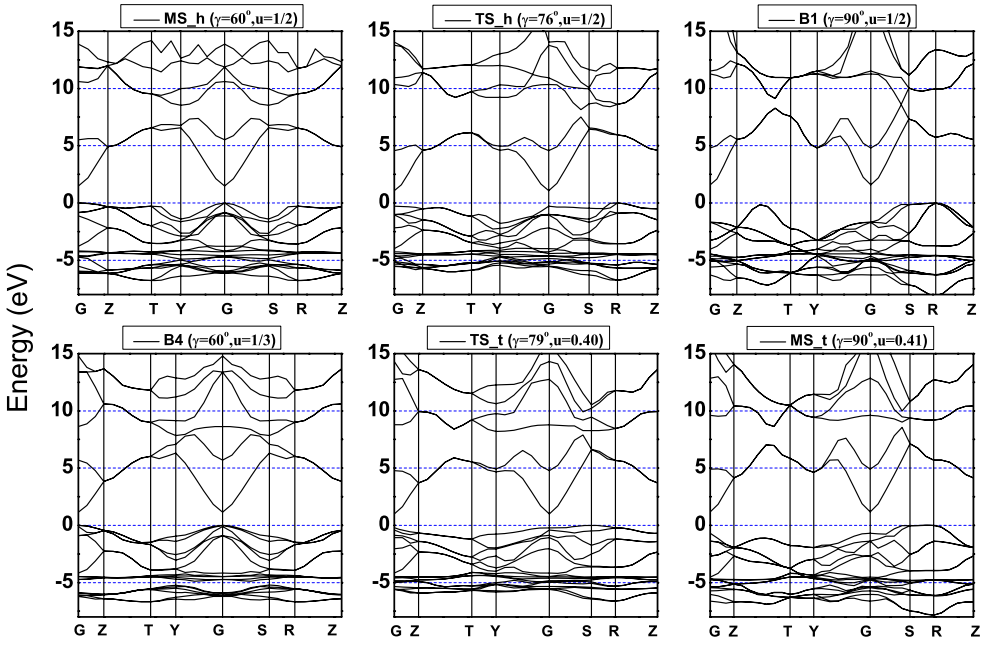

Figure 6. Electronic band structure of the B4, B1, and four representative intermediate states along the hexagonal and tetragonal transition paths based on DFT–LDA calculations under the transition pressure 8.4 GPa. Note that the state with the parameter ($\gamma = 90°$, $u = 0.41$) is not a metastable state at P_t but it is metastable at ambient pressure and 4.0 GPa (see table 2). For convenience, it is also referred to as MS_t here.

This observation implies that the band structures are strongly coupled with the strain (related to the angle γ) for the B4–B1 transition.

Second, it is well known that the energy band gaps are always underestimated by the Kohn–Sham eigenvalues because these do not truly represent quasiparticle excitation energies. The correction to the LDA gap is weakly dependent on the structure itself [34]. From the present calculated band structure, the band gap of B4-ZnO is estimated at 1.15 eV. Comparing it with the experimental gap of 3.4 eV [35], we can introduce a correction of 2.25 eV to apply

for the other structures. Including this correction, the gap of B1-ZnO is about 3.84 eV, which is still smaller than the theoretical value 4.51 eV [36] using the so-called GW approximation calculations; and the predicted gaps of ZnO in the intermediate structures of MS_h, TS_h2, TS_t1, and MS_t are 3.73, 3.32, 3.24, and 3.43 eV, respectively.

Now, considering that the electronic band structures are directly related to some of the optical properties, one might suggest measuring optical properties (e.g. absorption/transmission measurements) to acquire some knowledge about the transition path [20]. However, the present DFT–LDA calculated results show that the electronic band structure of the intermediate phases along the two possible transition paths mainly gives information related to the angle γ. In other words, the present results may not show obvious evidence to expediently identify the hexagonal or tetragonal path from the related measurement of optical properties. It is worth confirming this point by a precise description of the electronic properties with a better treatment of many-body effects, for example, using the GW approximation.

4. Conclusions

In summary, we have reported the first-principles calculated results on the microscopic mechanism for the B4–B1 phase transition of ZnO. There are two different transition paths proposed for the B4–B1 transition in recent studies, that is the hexagonal and the tetragonal paths. We firstly made a comparative study of these two paths from the energetic point of view. The calculated potential energy surfaces of ZnO at various pressures were taken as a basis to select or to determine the energy-favoured transition path. Our calculated results show that the hexagonal and the tetragonal paths are competitive in the ZnO case, which is significantly affected by the external pressure. In other words, the tetragonal path is preferred in the lower pressure range but the hexagonal one is preferred in the higher pressure range. This kind of pressure dependence might be very important in solving the arguments on the B4–B1 transition mechanisms. However, the preferences of the two transition paths under different pressures do not agree with the analysis results given in a recent experimental work. So, there are still unsettled questions left for both the experimental and theoretical studies. To shed light on this issue, we have carried out preliminary work to investigate the evolution of structural and electronic properties along the two different transition paths. The calculated results suggest the axial ratio c/a as a good indicator to distinguish between the hexagonal and the tetragonal paths in experiments. Also, we made an interesting observation that the band structures of ZnO for the different intermediate states of the B4–B1 transition are mainly dependent on the cell angle γ. The present study is also significant for the understanding of the B4–B1 transition commonly observed in many other wurtzite semiconductor compounds.

Acknowledgments

This work was supported by the National Natural Science Foundation of China (Grant No. 50531050) and the 973 Project in China (Grant No. 2006CB605100).

References

[1] Nomura K, Ohta H, Ueda K, Kamiya T, Hirano M and Hosono H 2003 *Science* **300** 1269
[2] Huang M H, Mao S, Feick H, Yan H, Wu Y, Kind H, Weber E, Russo R and Yang P 2001 *Science* **292** 1897
[3] Lee C T, Su Y K and Wang H M 1987 *Thin Solid Films* **150** 283
[4] Bates C, White W and Roy R 1962 *Science* **137** 993
[5] Decremps F, Zhang J and Liebermann R C 2000 *Europhys. Lett.* **51** 28

[6] Karzel H, Potzel W and Kofferlein M 1996 *Phys. Rev.* B **53** 11425
[7] Desgreniers S 1998 *Phys. Rev.* B **58** 14102
[8] Decremps F, Zhang J, Li B and Liebermann R C 2001 *Phys. Rev.* B **63** 224105
[9] Decremps F, Datchi F, Saitta A M, Polian A, Pascarelli S, Cicco A D, Itié J P and Baudelet F 2003 *Phys. Rev.* B **68** 104101
[10] Wu X, Wu Z, Guo L, Liu C, Liu J, Li X and Xu H 2005 *Solid State Commun.* **135** 780
[11] Recio J M, Blanco M A, Luaña V, Pandey R, Gerward L and Olsen J S 1998 *Phys. Rev.* B **58** 14
[12] Jaffe J E and Hess A C 1993 *Phys. Rev.* B **48** 7903
[13] Ahuja R, Fast L, Eriksson O, Wills J M and Johansson B 1998 *J. Appl. Phys.* **83** 8065
[14] Sun J, Wang H, He J and Tian Y 2005 *Phys. Rev.* B **71** 125132
[15] Seko A, Oba F, Kuwabara A and Tanaka I 2005 *Phys. Rev.* B **72** 24107
[16] Corll J A 1967 *Phys. Rev.* **157** 623
[17] Tolbert S H and Alivisatos A P 1995 *J. Chem. Phys.* **102** 4642
[18] Sharma S M and Gupta Y M 1998 *Phys. Rev.* B **58** 5964
[19] Knudson M D and Gupta Y M 1998 *Phys. Rev. Lett.* **81** 2938
[20] Knudson M D, Gupta Y M and Kunz A B 1999 *Phys. Rev.* B **59** 11704
[21] Limpijumnong S and Lambrecht W R L 2001 *Phys. Rev. Lett.* **86** 91
[22] Wilson M and Madden P A 2002 *J. Phys.: Condens. Matter* **14** 4629
[23] Limpijumnong S and Jungthawan S 2004 *Phys. Rev.* B **70** 54104
[24] Saitta A M and Decremps F 2004 *Phys. Rev.* B **70** 35214
[25] Sowa H 2001 *Acta Crystallogr.* A **57** 176
[26] Sowa H 2005 *Acta Crystallogr.* A **61** 325
[27] Shimojo F, Kodiyalam S, Ebbsjo I, Kalia R K, Nakano A and Vashishta P 2004 *Phys. Rev.* B **70** 184111
[28] Kresse G and Furthmüller J 1996 *Comput. Mater. Sci.* **6** 15
[29] Vanderbilt D 1990 *Phys. Rev.* B **41** 7892
[30] Monkhorst H J and Pack J D 1976 *Phys. Rev.* B **13** 5188
[31] Pendás A M, Luaña V, Recio J M, Flórez M, Francisco E, Blanco M A and Kantorovich L N 1994 *Phys. Rev.* B **49** 3066
[32] Bader R F W 1962 *Can. J. Chem.* **40** 1164
[33] Liu H, Ding Y, Somayazulu M, Qian J, Shu J, Häusermann D and Mao H 2005 *Phys. Rev.* B **71** 212103
[34] Limpijumnong S and Lambrecht W R L 2001 *Phys. Rev.* B **63** 104103
[35] Hellwege K-H and Madelüng O (ed) 1987 *Landolt–Börnstein New Series* Group III, vol 22a (Berlin: Springer)
[36] Ni H Q, Lu Y F and Ren Z M 2002 *J. Appl. Phys.* **91** 1339